JOURNAL OF SOLID STATE CHEMISTRY 116, 355–363 (1995)

Mixed Valent Nickel and Manganese Oxide Ceramics—Model Systems with Superconducting Properties?[1]

D. Reinen,[2] U. Kesper, and D. Belder

Fachbereich Chemie and Zentrum für Materialwissenschaften, Philipps-Universität, Hans-Meerwein-Straße, D-35043 Marburg, Germany

Received July 8, 1994, in revised form November 9, 1994; accepted November 11, 1994

Various oxidic solids of the perovskite and K_2NiF_4 type with Mn(III) and low-spin Ni(III) have been synthesized with clear structural and spectroscopic evidence for strong vibronic Jahn-Teller interactions. In the latter case clustering seems to induce a change to the high-spin state. In mixed valent Mn(III)/Mn(IV) compounds the Jahn-Teller effect is suppressed by band-broadening effects above a critical Mn(IV) concentration. Mixed valence Ni(III)/Ni(IV) ceramics could also be prepared, in which the positive hole is presumably located predominantly on the oxygen ligands, however. Superconducting properties are not observed down to 4 K. The possible significance of a strongly Jahn-Teller unstable *E* ground state, which occurs in the cases of Cu^{2+}, Mn^{3+}, and low-spin Ni^{3+} in octahedral coordination, for the appearance of superconductivity is discussed. © 1995 Academic Press, Inc.

I. INTRODUCTION

Mixed valent transition metal oxides, in which the lower oxidation state represents a Jahn-Teller unstable electron configuration, seem to be essential for generating superconducting properties. Well-established examples are compounds containing Cu^{2+} with a ^2E_g ($t_{2g}^6e_g^3$) ground state in combination with Cu(III), as the classical superconductor $La_{2-x}Sr(Ba)_xCuO_4$ (1). Concerning the electronic state of Cu(III) in this type of compound it is a still unsettled problem, whether Cu^{3+} is really present or Cu^{2+}, with charge-compensating electron holes in the ...ond bonding band of predominant oxygen character. The former alternative is more probable in the case of ...pounds, in which the Cu(III) centers are isolated ... each other in the structure, while a charge transfer ... state seems to be present, if electronic interac... between neighboring Cu(III) cations in the lattice ... involved (2). In the very few examples of oxidic cop... solids with a well-documented (+III) oxidation state square planar coordination and diamagnetism is ob... (D_{4h}: $^2A_{1g}$ ($e_g^4b_{2g}^2a_{1g}^2$) ground state)) (3). Here the Δ/B ratio (Δ and B, ligand field and Racah parameter of interelectronic repulsion, respectively) is large enough to induce the low-spin configuration, in contrast to elpasolite-type compounds A_2BCuF_6 (*A*: Cs; *B*; K, Rb), in which Cu^{3+} possesses a high-spin ground state $^3A_{2g}$ ($t_{2g}^6e_g^2$) and a regular octahedral coordination (4).

It seemed worthwhile to us to check experimentally whether oxidic ceramics with transition ions having comparable electronic properties to the Cu^{2+}/Cu^{3+} pair would exhibit superconductivity as well. As suitable model systems, mixed valent compounds with Ni^{3+}/Ni^{4+} and Mn^{3+}/Mn^{4+} were chosen. Low-spin Ni^{3+} has a ^2E_g ($t_{2g}^6e_g^1$) ground state in octahedral coordination similar to Cu^{2+} and vibronic Jahn-Teller coupling again induces a strong tetragonal elongation (5, 6). The difference is that the unpaired electron resides in a $d_{x^2-y^2}$ orbital in the case of Cu^{2+}, while it occupies a d_{z^2} orbital in low-spin Ni^{3+} compounds. For Mn^{3+} the same arguments hold, the ground state being a spin quintet, however: ^5E_g ($t_{2g}^3e_g^1$). The generation of holes leads to low-spin Ni(IV), $^1A_{1g}$ (t_{2g}^6), and Mn(IV), $^4A_{2g}$ (t_{2g}^3).

II. EXPERIMENTAL SECTION

A. Manganese (Chromium) Oxide Ceramics

(a) $Sr_2Zn_{1-x}Mn_xTe_{1-x}Sb_xO_6$ solid solution. The mixed crystals were prepared from homogenous mixtures of $SrCO_3$, $Zn(NO_3)_2$, Mn_2O_3, Sb_2O_3, and Te in the appropriate molar ratios, which were heated in oxygen with a rate of 100°C/hr to the final temperature and held at this temperature for 12 to 15 hr. In some cases it was necessary to repeat the sintering procedure under the same conditions after mortaring. The final temperatures were 1100°C for $x \leq 0.4$ and 1250 to 1300°C for $x \geq 0.55$. There seems to be a miscibility gap around $x \approx 0.50$.

(b) $Sr_2Zn_{0.2}Ga_{0.8-x}Mn(Cr)_xTe_{0.2}Sb_{0.8}O_6$ solid solution. The preparation method followed that under (a)—$Ga(NO_3)_3$ was used additionally as initial compound. The final sintering temperatures were 1250 to 1300°C for $x <$ 0.4 and 1200°C for $x \geq 0.4$.

Dedicated to Professor Hans-Uwe Schuster (University of Cologne, ...) on the occasion of his 65th birthday, in memoriam.

... whom correspondence should be addressed.

0022-4596/95 $6.00

Copyright © 1995 by Academic Press, Inc.

The corresponding chromium mixed crystals were synthesized analogously.

(c) *$Sr_2Zn_{0.2}Ga_{0.8-x}Mn(Cr)_xW_{0.2}Ta_{0.8}O_6$ solid solution.* Again the preparation procedure was that described in (a). In most cases a second sintering period after thorough mortaring was necessary, however.

(d) *$SrNdGa_{1-x}Mn_xO_4$ mixed crystals.* The initial mixtures of $SrCO_3$, Nd_2O_3, $Ga(NO_3)_3$, and Mn_2O_3 were heated in flowing argon at 1370°C for 12–15 hr. After thorough mortaring a second sintering procedure was performed under the same conditions.

(e) *$Sr_{1+x}Nd_{1-x}MnO_4$ solid solution.* The synthesis followed that under (d), but in the initial mixture MnO_2 was used additionally in the appropriate molar amount.

The average oxidation states of manganese in the investigated compounds—as obtained by calibrated iodometric analyses—are the following, the experimental error being about 2%:

(a) to (d) 3.0 ± 0.1 (Sb(V) also oxidizes I^-)

(e) $3 + x \pm 0.15$.

If the deviation from the expected oxidation state was larger than ±0.1 or ±0.15 in case (e) the respective compound was newly synthesized.

B. Nickel Oxide Ceramics

(a) *$LaSrGa_{1-x}Ni_xO_{4-\delta}$ solid solution.* Stochiometric mixtures of the metal nitrates ($La(NO_3)_3$ and $Ni(NO_3)_2$ in aqueous solution) were evaporated to dryness and decomposed at 700°C in flowing oxygen. After homogenization by mortaring, the powders were heated for 24 hr in oxygen at 1000°C (cooling rate 100°/hr). The compounds were finely mortared again and sintered a second time in flowing oxygen (60 hr, 1200°C; cooling rate 100°/hr). The iodometric analyses indicate oxygen deficiency.

(b) *$La_{1-x}Sr_{1+x}NiO_{4-\delta}$ solid solution.* The mixed crystals were synthesized from $La(OH)_3$, $SrCO_3$, and $NiCO_3$ as homogeneous mixtures by heating in an oxygen flow for 12–15 hr at 1200°C. After mortaring a second sintering period under the same conditions followed. Pure compounds were only obtained up to $x \approx 0.5$ with δ values near to zero (iodometric analyses).

C. Experimental Techniques

(a) The purity of the solid solutions was checked by X ray diffractometry. The unit cell parameters were determined from calibrated Guinier diagrams.

(b) The UV/VIS spectra were measured using the powder reflection technique. EPR spectroscopy was performed at X and Q band frequencies and in the temperature range between 300 and 4K using a Bruker spectrometer.

III. RESULTS AND DISCUSSION

A. The Jahn-Teller Effect of Mn^{3+} in Oxide Ceramics

To our knowledge no detailed investigations concerning Jahn-Teller distortions of Mn^{3+} in an octahedral oxide coordination have been reported thus far, in contrast to fluorides, whose *d–d* spectra have been analyzed thoroughly (7). Three examples will be given subsequently.

Mn^{3+} in perovskite-type solids. Figure 1 nicely demonstrates the presence of a Jahn-Teller distortion caused by Mn^{3+}. With increasing concentration of the latter cation the tetragonal distortion of the perovskite-type lattice steadily increases. We have used a solid $Sr_2(Ga_{0.8}Zn_{0.2})^B(Sb_{0.8}Te_{0.2})^BO_6$ of rather complex constitution as the host compound in order to introduce cation ordering on the octahedral sites. While $Sr_2Ga^{III}Sb^VO_6$ is a disordered perovskite, the presence of about 20 mole% Te(VI) and Zn(II) introduces ordering due to the enhancement of the charge difference between sites *A* and *B*. Ga^{3+} has been chosen as the cation to be substituted because of its radius (0.62 Å) being similar to that of (high-spin) Mn^{3+} (0.65 Å) (8). The octahedral positions in $Sr_2(Zn_{0.2}Ga_{0.8}$ $(Sb_{0.8}Te_{0.2})O_6$—the structure slightly deviates from cubic but could not be characterized even by analyzing the Guinier diagrams due to rather broad reflections—seem to be slightly deformed, locking the Mn^{3+} cations into a static distortion by lattice strains even at low *x* values.

Similar observations are made for mixed crystals $Sr_2Zn_{1-x}Mn_x^{III}$ $Te_{1-x}Sb_xO_6$ above the critical concentration of $x_c \approx 0.5$ (Fig. 2). Though the host compound ($x = 0$) is distorted ($a \approx 7.962$ Å, $c \approx 7.924$ Å, $\beta \approx 90°18'$)

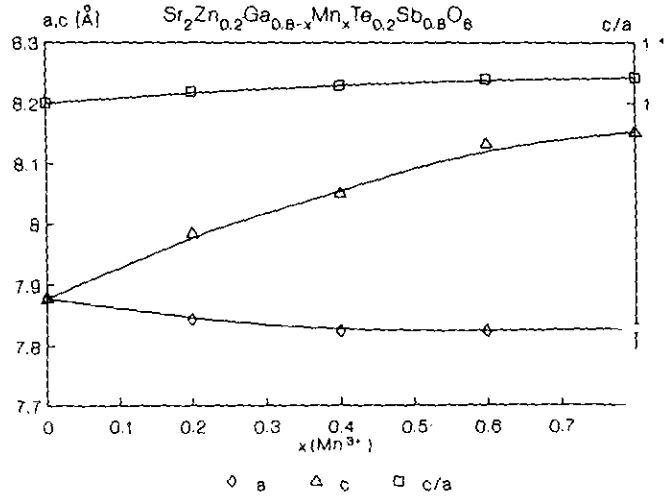

FIG. 1. Unit cell constants and *c/a* ratios of elpasolite-type crystals $Sr_2(Ga_{0.8-x}Mn_x{}^{III}Zn_{0.2})(Sb_{0.8}Te_{0.2})O_6$ (The unit cell parameters of the tetragonal phases has been enlarged to $a = a'\sqrt{2}$ in order to a comparison with cubic lattice constants).

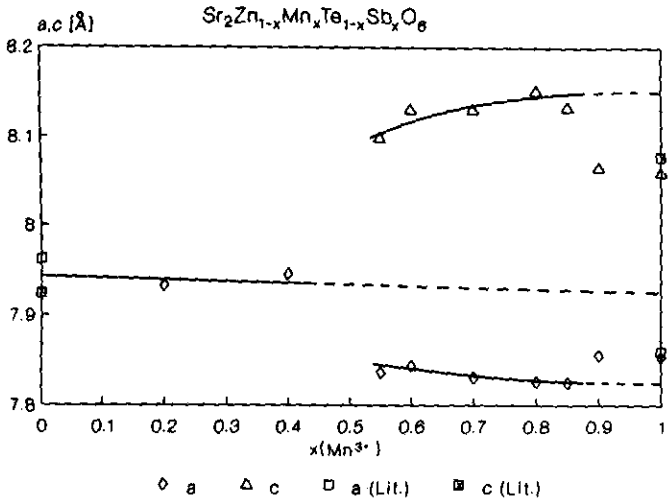

FIG. 2. Unit cell parameters of perovskite-type mixed crystals $Sr_2Zn_{1-x}Mn_x^{III}Te_{1-x}Sb_xO_6$ (see (9, 10) for unit cell parameters for $x = 0$ and $x = 1$, respectively; cation order disappears above $x \approx 0.85$; the unit cell parameter a' of the tetragonal phases has been enlarged to $a = a'\sqrt{2}$ in order to allow a comparison with cubic lattice constants.)

(9) the octahedral sites are apparently nearly regular,[3] thus allowing the local Jahn-Teller distortion to be dynamic at $x < x_c$. The compounds are ordered only up to $x \approx 0.85$ (see the argument in the preceeding paragraph), and it is interesting to note that the c/a ratio discontinuously decreases if the elpasolite transforms to the perovskite structure (Fig. 2). As is well known (6, 11) the local Jahn-Teller distortion is drastically reduced if high-valent cations (M = (Sb^{5+}, Te^{6+}) occupy the same sites as the vibronically unstable ions—due to elastic forces, which try to keep the MO_6 octahedra undistorted.

As expected the cooperative order of elongated MnO_6 octahedra is ferrodistortive, the pattern of which allows the octahedral sites occupied by Te(VI), Sb(V) to remain regular in the elpasolite lattice (6). From the unit cell parameters between $x = 0.4$ and 0.6 (Fig. 1) and between $x = 0.55$ and 0.8 (Fig. 2) and using available ionic radii (8) a considerable local distortion of the MnO_6 octahedra with Mn–O spacings of about 1.95 Å (4x) and 2.25 Å (2x) is roughly estimated. In the disordered perovskite phases all octahedral sites have to deform to a similar extent, the resisting elastic influence of the high-valency cations inducing a reduced local Jahn-Teller distortion, as mentioned.

The elpasolite-type mixed crystals are grayish at low and black at high x values, due to charge-transfer bands which seem to overlap the d–d transitions. A band structure is indicated by a continuous absorption, which finally extends to rather low energies far into the IR region (Fig. 3). In contrast the corresponding cubic mixed crystals $Sr_2(Zn_{0.2}Ga_{0.8-x}Cr_x)(Te_{0.2}Sb_{0.8})O_6$ ($x = 0.2$, $a = 7.90_5$ Å; $x = 0.8$, $a = 7.87$ Å) with Cr^{3+} have pink to violet colors between $0 < x \leq 0.8$ with well-resolved d–d transitions at 13,200 cm^{-1} ($^4A_{2g} \rightarrow {}^4T_{2g}$) and 19,000 cm^{-1} ($^4A_{2g} \rightarrow {}^4_aT_{1g}$), from which the ligand field parameters $\Delta \approx$ 13,200 cm^{-1} and $B \approx 580$ cm^{-1} are derived (Fig. 3). The spectroscopic results indicate that the Mn(III)–O bond is more covalent than the Cr(III)–O bond, leading to stronger delocalization effects in the former case. Electron delocalization of this extent is not really expected, because the cation ordering induces rather large $Mn^{3+}(Cr^{3+})$–$Mn^{3+}(Cr^{3+})$ distances of $\approx$ 5.5 Å. Apparently only bonding MO's of predominantly oxygen character broaden into bands in the case of Mn(III), however. The antibonding d–MO's seem to be essentially localized even in the case of Mn^{3+}, because local vibronic coupling effects of the Jahn-Teller type are still observed, which would be suppressed in the case of e_g^* broad band behavior (see below).

It is interesting to compare the above results with elpasolite-type mixed crystals $Sr_2(Zn_{0.2}Ga_{0.8-x}M_x)(W_{0.2}Ta_{0.8})O_6$ ($M = Cr^{3+}$, Mn^{3+}), in which the d^{10} configurated Sb(V) and Te(VI) cations are substituted by Ta(V) and W(VI) with a d^0 configuration. The Mn(III) mixed crystals are brownish-black to black, and the same phe-

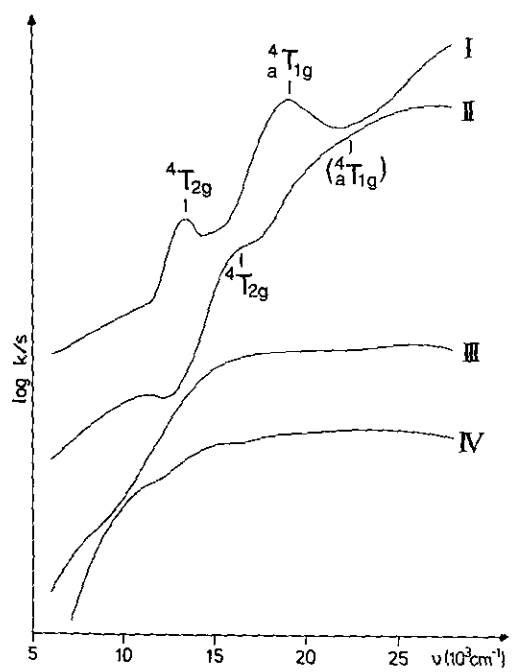

FIG. 3. Diffuse reflectance spectra (298 K, intensity in arbitrary units) of elpasolite-type compounds $Sr_2(Ga_{0.6}M^{III}_{0.2}Zn_{0.2})(Sb_{0.8}Te_{0.2})O_6$ (M^{III}: Cr^{3+} (I), Mn^{3+} (III)) and $Sr_2(Ga_{0.6}M^{III}_{0.2}Zn_{0.2})Ta_{0.8}W_{0.2}O_6$ (M^{III}: Cr^{3+} (II), Mn^{3+} (IV)). The d–d transitions for Cr^{3+} ($^4A_{2g}$ ground state) are indicated.

[3] The lattice distortion is presumably caused by small cooperative rotations of neighboring octahedra around the c_4 axis $\parallel c$ in the opposite direction—neglecting the tiny monoclinic component.

nomenon of charge-transfer bands superimposing the d–d transitions even at rather low concentrations is observed (Fig. 3). It is interesting to note, that—in contrast to the situation in the Sb(V)–Te(VI) elpasolites—the compounds remain cubic even at the highest Mn^{3+} concentration ($x = 0$, $a = 7.91_5$ Å; $x = 0.8$, $a = 7.93$ Å). Apparently W(VI)/Ta(V) with their empty d shells are more effective in transfering electron density than Te(VI)/Sb(V). We hence suppose that the Jahn-Teller effect is suppressed, as predicted by Höck *et al.* (12) for the case that the width of the antibonding e_g^* band is larger than the possible splitting as a consequence of vibronic Jahn-Teller coupling (see also Section III.B). The chromium compounds ($x = 0.2$, $a = 7.89_5$ Å; $x = 0.8$, $a = 7.87$ Å) possess brown colors due to charge-transfer bands in the visible region of the optical spectrum, only revealing the first $^4A_{2g} \rightarrow {}^4T_{2g}$ d–d-transition as a shoulder at low x values ($\Delta \approx 16{,}500$ cm^{-1}; Fig. 3). We interpret this behavior again as caused by a more extensive d-electron delocalization. Different M–O bonding properties in the Sb(V), Te(VI) and Ta(V), W(VI) compounds, respectively, are also indicated by the ligand field parameter Δ in the case of Cr^{3+}, which is by about 25% larger for the elpasolites with d^0 than for those with d^{10} cations. Similarly Ni^{2+} in Sr_2NiTeO_6 for example has a considerably lower Δ value than in the corresponding compound Sr_2NiWO_6. The origin has been discussed elsewhere on the basis of the interplay between σ- and π-interactions in the Ni(II)–O–W(VI) (Te(VI)) fragments (13).

Mn^{3+} in K_2NiF_4-type solids. Furthermore we investigated K_2NiF_4-type mixed crystals $SrNdGa_{1-x}Mn_xO_{4+\delta}$. They were prepared by carefully controlling the oxidation state of manganese. The iodometric analyses yielded values of 3.1 ± 0.1 ($-0.1 \lesssim 2\delta \lesssim 0.1$). Consistent with the results comprised in Figs. 1 and 2 the c/a ratio increases with increasing Mn^{3+} concentration (Fig. 4). We estimate Mn–O spacings in $SrNdMnO_4$ of about 1.885 Å ($4x$) and 2.275 Å ($2x$), using the lattice constant $a \approx 3.77$ Å and an average Mn–O bond length of 2.015 Å (8). They are nearly identical with those derived from a single-crystal structure analysis (1.89 and 2.28 Å (15)). The local polyhedron distortion is rather large, because the Jahn-Teller contribution adds to the already existing host site elongation. Thus the Ga–O bond lengths in $SrNdGaO_4$ are estimated to be—with $a \approx 3.82$ Å and an average Ga–O spacing of 1.99 Å (8)–1.91 Å ($4x$) and 2.15 Å ($2x$). This considerable host site distortion may be explained as originating from the contrapolarizing force of the comparatively small Nd^{3+} cations on the axial oxygen ions (see Fig. 11). The mixed crystals are black and the charge-transfer region extends down to about 13,000 cm^{-1} already at very low Mn^{3+} concentration, indicating extensive electron delocalization. This is expected because the MnO_6 octahedra are corner-connected in the equatorial plane of the K_2NiF_4 structure. The ground state splitting should be larger than that in the perovskite-type compounds (Figs. 1, 2) by about 30%—as one may deduce by using the appropriate formalism (11)—due to the additional contribution by the host site strain (see above).

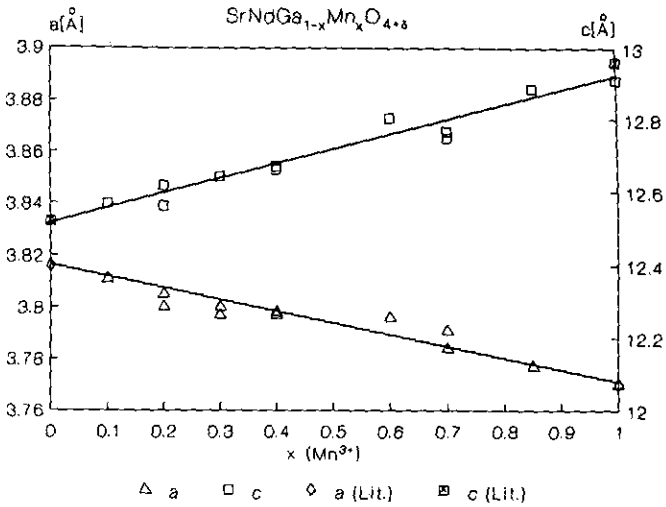

FIG. 4. Unit cell parameters of mixed crystals $SrNdGa_{1-x}Mn_xO_{4+\delta}$ (Literature: $x = 0$ (14), $x = 1$ (15); for most x values unit cell parameters for two different preparations are reported, which differ with respect to the oxidation state of Mn within the given limits).

We may conclude from these results, that the $a_{1g}^*(d_{z^2})$ and b_{1g}^* $(d_{x^2-y^2})$ states of Mn^{3+}—originating from the octahedral e_g^* parent states—are not very broad in the investigated oxidic Mn^{3+} solids. Even in the K_2NiF_4 solids, where the Mn^{3+} centers occupy neighboring sites connected by common oxygen ligands, the width in particular of the strongly antibonding b_{1g}^* $(d_{x^2-y^2})$ band is apparently not large enough to suppress the Jahn-Teller coupling.

B. Mn(III)/Mn(IV) Mixed Valence Ceramic Oxides

We succeeded in preparing the complete mixed crystal series $Sr_{1+x}Nd_{1-x}MnO_{4+\delta}$ with the K_2NiF_4 structure. The differences between the experimental oxidation states and those expected for $\delta = 0$ vary between ± 0.15, corresponding to $0.15 > 2\delta > -0.15$. The a and c unit cell parameters have a rather complex dependence on the ratio between Mn(III) and Mn(IV) (Fig. 5). In particular the c parameters scatter due to the deviations of the manganese oxidation states from the expected value for $\delta = 0$. It is possible for example to synthesize a pure phase $SrNdMnO_{4.12}$, in which manganese possesses an average oxidation state of $= 3.14$. The lattice constants ($a = 3.82_0$ Å; $c = 12.55$ Å) are very similar to those of $Sr_{1.2}Nd_{0.8}MnO_4$ with manganese having a similar oxidation state.

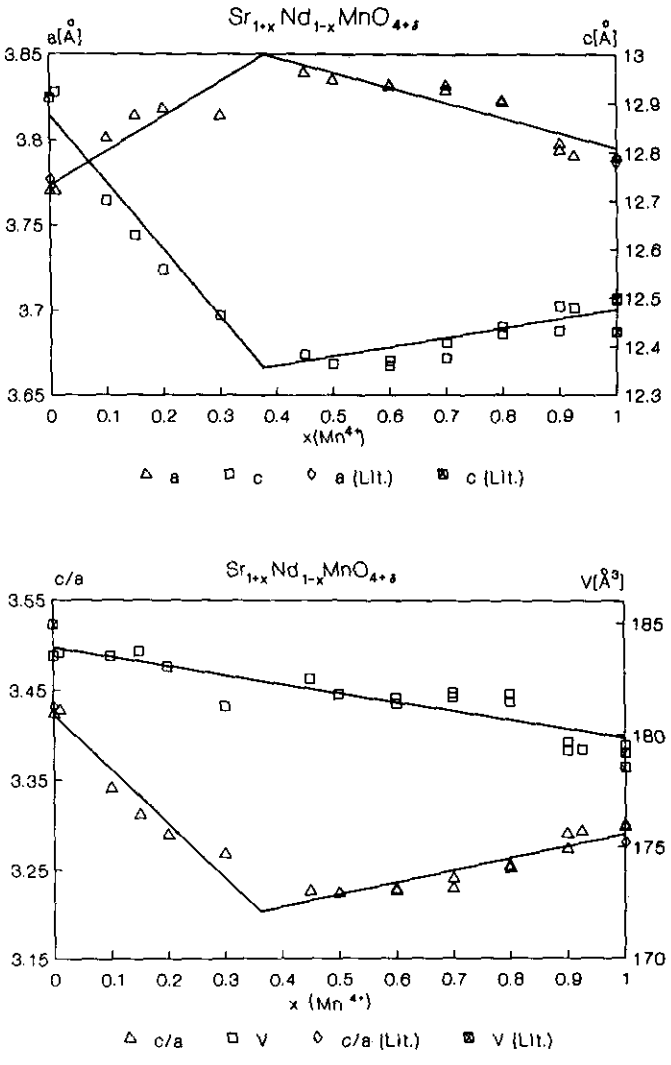

FIG. 5. Unit cell parameters (a, c; c/a, unit cell volume V) of mixed crystals $Sr_{1+x}Nd_{1-x}MnO_{4+\delta}$ (Literature: $x = 0$ (15), $x = 1$ (16); most compounds have been prepared twice, with differences between the structural parameters due to variations in the oxidation states within the range ±0.15]

One would have expected a linear decrease of c and increase of a between $x \approx 0$ and 1.0, continuously reducing the octahedral site distortion by raising the manganese oxidation state from 3 to 4, because Mn^{4+} with a $^4A_{2g}$ ground state is not Jahn-Teller active—in analogy to Fig. 3. In contrast the minimum c and maximum a values are already reached at $x \approx 0.4$, indicating that the Jahn-Teller vibronic coupling due to the presence of Mn^{3+} is already completely quenched at this critical concentration. We indeed estimate from the a lattice constant and the appropriate ionic radii (8) for the compound with $x = 0.5$ only slightly differing Mn–O spacings of ≈ 1.92 Å (4x) and ≈2.04 Å (2x), the remaining distortion being definitely caused by lattice strains.[4] The decrease of a (≈0.05 Å) and increase of c (≈0.15 Å) between $x \approx 0.4$ and $x = 1.0$ exclusively reflects the ionic radii effects by the substitution of Mn^{3+} by Mn^{4+} and of Nd^{3+} by Sr^{2+}, respectively. The small decrease of the unit cell volume with increasing x reflects the mentioned coupled substitution—but cannot be verified on the basis of the available ionic radii (8).

The suppression of the local Jahn-Teller distortion on the Mn^{3+} sites at $x \approx 0.37(1)$ (Fig. 4) can be explained by electron delocalization induced by the presence of the more covalent Mn^{4+} ion, broadening the antibonding e_g^* band such that the band width becomes larger than the Jahn-Teller splitting. To our knowledge this is the first well-documented example in literature proving the validity of the theorem by Höck *et al.* (12) for transition metal ceramic solids.

All mixed crystals are deeply black, with a continuous absorption extending into the infrared spectral region. The magnetic properties between 4 and 300 K give no indication of superconductivity and will be reported separately, together with the results of neutron diffraction studies of two mixed crystals with the purpose of analyzing whether it is possible to distinguish between Mn(III) and Mn(IV) within the time scale of the chosen diffraction methods (17).

C. The Jahn-Teller Effect of Ni^{3+} in Oxide Ceramics with the K_2NiF_4 Structure

The average oxidation states of mixed crystals $LaSrGa_{1-x}Ni_xO_{4-\delta}$ (18) vary from about 2.4 at low to ≈2.8 at high x values, indicating the presence of Ni^{2+} and oxygen deficiencies up to $\delta \approx 0.1$ (Fig. 6). The EPR spectra reveal the presence of high-spin and low-spin Ni^{3+} side by side (Fig. 7), the former giving rise to an anisotropic signal at g values between 4 and 7 and the latter to a spectrum characteristic of a d_z^2 ground state and a tetragonally elongated octahedron. The high-spin/low-spin intensity ratio strongly increases with x becoming larger, up to the critical concentration for the observation of an EPR spectrum at $x \approx 0.3$. The room temperature magnetic moments in the range $0 < x < 0.2$ are 2.85 ± 0.15 μ_B, the values of which are rather those characteristic of Ni^{2+}. Above $x \approx 0.3$ the moments steadily decrease to 1.45 μ_B for $x = 1.0$, due to exchange interactions. In

[4] The host site deformation in Sr_2MnO_4 ($a = 3.79$ Å; $c = 12.47$ Å) is presumably nearly vanishing (Mn(IV)–O spacings: ≈1.895 Å (4x) and ≈1.91 Å (2x)), because the contrapolarizing force of the rather large Sr^{2+} ion is not very effective. Hence the estimated site distortion in $Sr_{1.5}Nd_{0.5}MnO_4$ is expected to be intermediate between those of Sr_2MnO_4 and $SrNdGaO_4$ (see Section III.A), if electronic effects of vibronic Jahn-Teller type are absent—in agreement with the experimental finding.

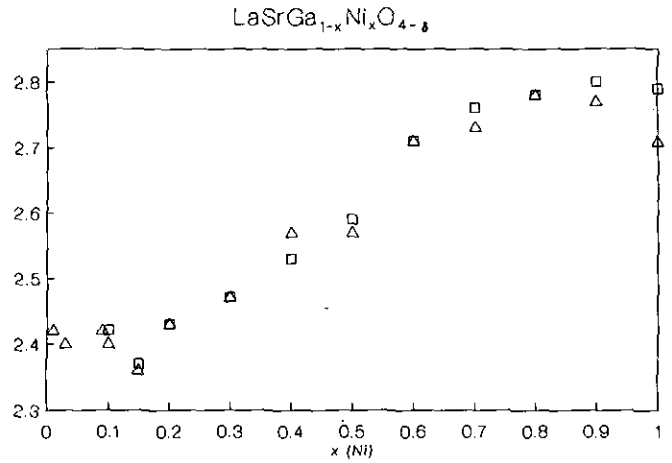

FIG. 6. Average oxidation states of nickel in mixed crystals $LaSrGa_{1-x}Ni_xO_{4-\delta}$ (the squares represent solids, which were treated with oxygen at 700°C in a second sintering procedure (see under Experimental)).

contrast the compound $La_2Li_{1/2}Ni_{1/2}O_4$ (19), which crystallizes in a K_2NiF_4 structure with an ordered cation distribution on the octahedral sites—the results of a single-crystal analysis will be reported elsewhere (20)—contains exclusively low-spin Ni^{3+}. The powder EPR spectrum is shown in Fig. 8, in comparison with the spectrum of $LaSrNi_{0.07}Ga_{0.93}O_4$ in the low-spin region.

Ni^{3+} in the octahedral fluoride environment of elpasolite-type compounds is low-spin configurated. Though in regular octahedral environments high-spin Ni^{3+} should be the energetically preferred electron configuration, it is actually the Jahn-Teller splitting 4 E_{JT} of the excited ^2E_g state which finally stabilizes a low-spin ground state (5, 6) (Fig. 9). For oxidic compounds as those under discussion the octahedral low-spin–high-spin separation energy δE_{HL} should be even smaller due to more strongly reduced parameters of interelectronic repulsion B, C, and a higher Δ value, but the vibronic Jahn-Teller coupling constant, which mainly determines the ground state splitting, is expected to be also smaller (11). The deviation of $g_\parallel$ from the spin-only value makes it possible to deduce the doublet–quartet energy separation $\delta_{2,4}$ (Fig. 9) from the EPR spectrum (Eq. [1]) (5). With an effective spin-orbit

$$g_\parallel = g_0 + 2(\zeta/\delta_{2,4})^2 \qquad [1]$$

coupling parameter $\zeta \approx 400$ cm^{-1} (5) we estimate for $La_2Li_{1/2}$ $Ni_{1/2}O_4$ a $\delta_{2,4}$ energy of about 5000 cm^{-1}, while in

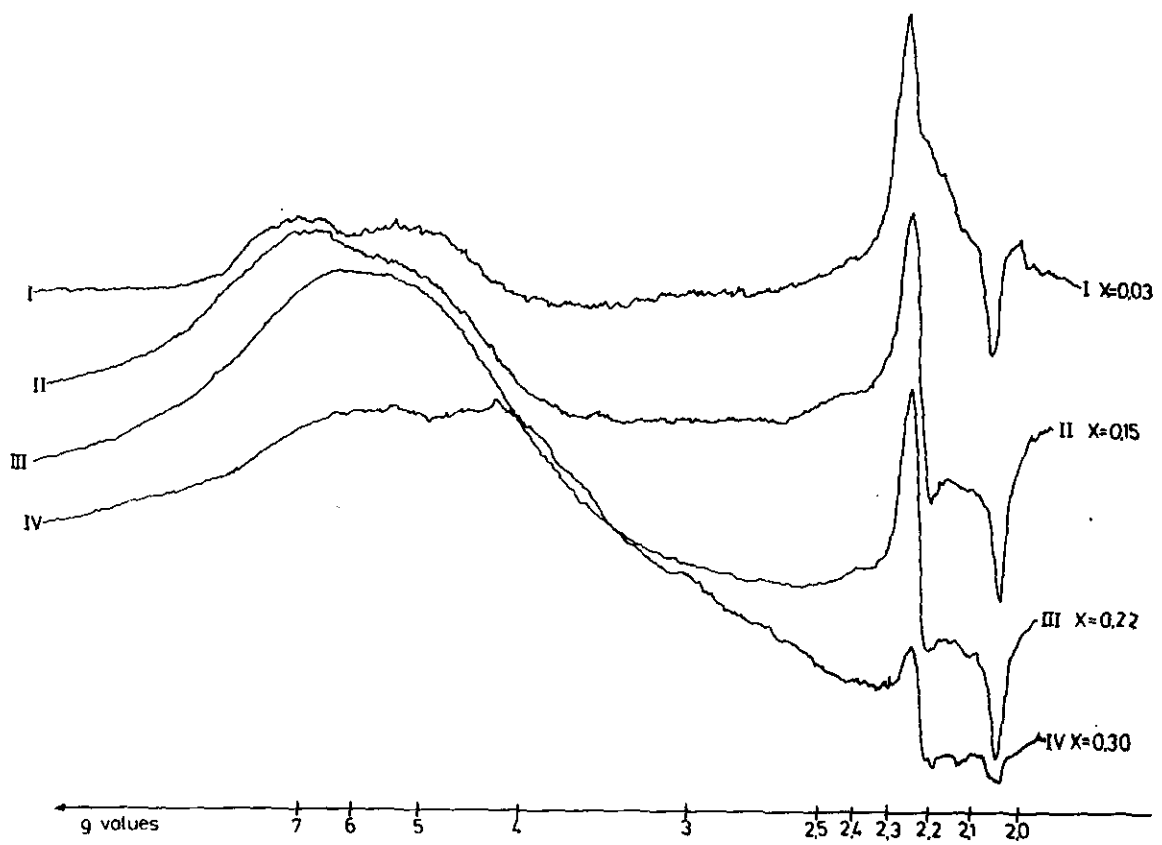

FIG. 7. EPR spectra (4.2 K, 34.9 GHz) of mixed crystals $LaSrGa_{1-x}Ni_xO_{4-\delta}$.

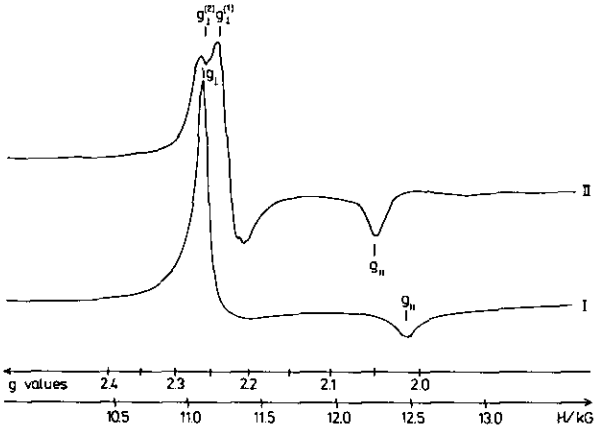

FIG. 8. EPR spectra (298 K, 35.3 GHz) of $La_2Li_{1/2}Ni_{1/2}O_4$ (I: $g_\parallel$ = 2.014, $g_\perp$ = 2.256) and $LaSrNi_{0.07}Ga_{0.93}O_4$ (II: $g_\parallel$ = 2.044, $g_\perp^{(1)}$ = 2.227, $g_\perp^{(2)}$ = 2.250).

the case of nickel-doped $LaSrGaO_4$ the energy would be $\approx$2500 cm^{-1}. The strong stabilization of the $^2A_{1g}$ ground state in the former compound has to be traced back to a very large ground state splitting due to a considerable NiO_6 polyhedron distortion with a difference of 0.40 Å between the long and short Ni–O spacings (20). The obvious reason is an already distinct host site distortion as the consequence of the contrapolarizing force of the La^{3+} cations on the axial oxygen ligator atoms (Fig. 11)—as discussed in Section III.B. In the mixed crystals $LaSrGa_{1-x}Ni_xO_{4-\delta}$ the contrapolarizing force is smaller due to the presence of Sr^{2+}, reducing the host site distortion and the ground state splitting, and hence inducing a smaller $\delta_{2,4}$ separation. The appearance of two $g_\perp$ signals (Fig. 8) will be discussed below.

We think that the low-spin signal (Fig. 7) originates from isolated Ni^{3+} centers in the $LaSrGaO_4$ matrix, while the high-spin signals are induced by broadening effects of the σ-antibonding a_{1g}^* (d_z^2) and in particular b_{1g}^* ($d_x^2 - y^2$) *MO*'s, connected with electronic interactions between nickel centers, occurring in clusters. If the bandwidth is larger or comparable to $\delta_{2,4}$ the high-spin is preferred with respect to the low-spin configuration (Fig. 9). This argument is consistent with the observation of a strong increase of the high-spin Ni^{3+} concentration with increasing x.

The dependence of the lattice parameters on the nickel concentration is shown in Fig. 10. Though the large per-

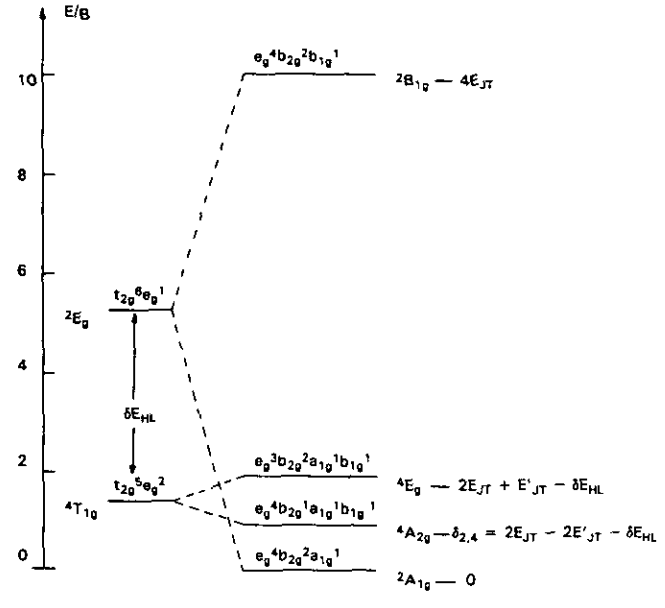

FIG. 9. Schematic energy diagram of an NiF_6^{3-} polyhedron (O_h and elongated D_{4h} coordination, lowest quartet and dublet terms; energies are those in the strong field approximation $-\delta E_{HL} \simeq 4B + 4C - \Delta$; E_{JT} and $E_{JT'}$: Jahn-Teller splitting parameters for σ- and π-antibonding e_g and t_{2g} states, respectively) with Δ/B = 18.5, C/B = 4.5, E_{JT}/B = 2.5, E'_{JT}/B = 0.33. e_g, b_{2g}, a_{1g}, and b_{1g} are the one-electron symmetry notations of the d orbitals in a D_{4h} environment.

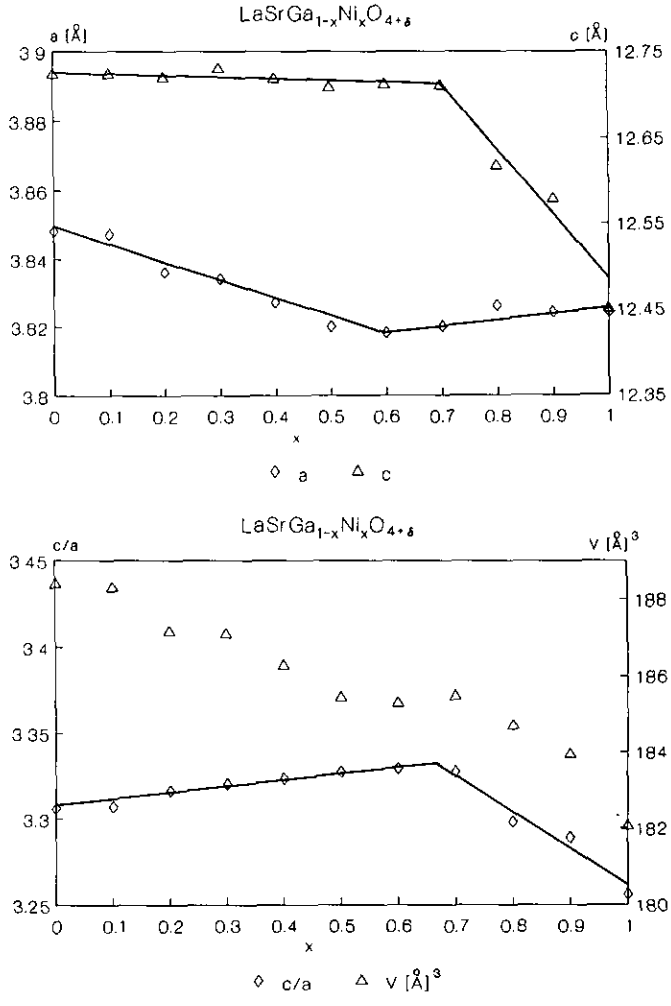

FIG. 10. Unit cell parameters (a, c; c/a, unit cell volume) of mixed crystals $SrLaGa_{1-x}Ni_xO_{4-\delta}$ (Literature, x = 1.0: a = 3.826 Å, c = 12.45 Å (19)).

centage of Ni^{2+} and the accompanying oxygen deficiency obscures a straight-forward argument, the increase of the c/a ratio up to $x \approx 0.7$ indicates the presence of Jahn-Teller elongated octahedra with low-spin Ni^{3+}, while the sharp decrease above this x value supports the argument of a finally complete low-spin-to-high-spin conversion. The ligand field spectra at lower x values are dominated by bands originating from octahedral Ni^{2+}.

Similar results to those reported are observed for mixed crystals $SrLaAl_{1-x}Ni_xO_4$ (21), which contain less Ni^{2+} than the corresponding Ga^{3+} compounds, however (22). The authors explain the appearance of two $g_\perp$ signals in the low-spin part of the EPR spectra of nickel-doped $LaSrAlO_4$ by the presence of two different sites. As one may deduce from Fig. 11, the equatorial and axial oxygen atoms of a BO_6 polyhedron in an A_2BO_4 unit cell with the K_2NiF_4 structure are approximately octahedrally coordinated by a B_2A_4 and BA_5 cationic environment, respectively. For reasons discussed above a preferential coordination either by Sr^{2+} or by La^{3+} should indeed induce different polyhedron distortions and ground state splittings. Though this idea seems to be attractive at the first sight, some arguments are in severe contrast to this assumption. First, no splitting of the $g_\parallel$ signal is observed, which is to be expected to be as significant as that of $g_\perp$, looking at the respective equations for $g_\parallel$ and $g_\perp$ in more detail (5, 6). Also no significant change in the intensity ratio between $g_\perp^{(1)}$ and $g_\perp^{(2)}$ is observed in dependence on x and switching from the Ga^{3+} to the Al^{3+} mixed crystal series—as far as this can be deduced from powder spectra simulations. Second, there is no evidence of a Sr^{2+}–La^{3+} long-range ordering in the powder Guinier diagrams. We also exclude short-range order, because the EPR signals of Cu^{2+} in a similar mixed crystal series $Sr_{1-x}La_{1+x}Ga_{1-x}Cu_xO_4$ do not show any splitting of the kind observed here (3). After all we propose that the origin of the two $g_\perp$ signals is a lower symmetry distortion component superimposed on the tetragonal D_{4h} elongation, which is expected from the combined action of vibronic Jahn-Teller coupling and the host site effect in the K_2NiF_4 structure. We think that the mentioned lower symmetry deformation is induced by the random strain due to the simultaneous presence of high-spin and low-spin Ni^{3+}, Ga^{3+}, and Ni^{2+} in the cationic coordination sphere of any low-spin Ni^{3+} center. We have also checked whether Ni^{2+} could induce EPR signals at $g \approx 2.25$. For this purpose we have synthesized mixed crystals $La_{1+x}Sr_{1-x}Ga_{1-x}Ni_xO_4$ which could be obtained as pure compounds for $x \gtrsim 0.4$, with oxidation states of ≈ 2.3 for nickel. The unit cell dimensions are independent of x ($a = 3.85_5$ Å, $c = 12.70$ Å) and very near to those reported for $LaSrGaO_4$ (3) and La_2NiO_4 (23). The EPR spectra did not show any sharp feature in the critical region, however, and the observed broad signals can be assigned as caused by zero-field splitting ($D \approx 2.5$ cm^{-1}, $g \approx 2.15$).

We conclude from the reported investigations that it is possible to stabilize Ni(III) in oxidic compounds. If they are isolated in the host structure, the low-spin configuration is stabilized. As soon as they are involved in cooperative electronic interactions with each other, a band structure evolves and the low-spin switches to a high-spin ground state.

D. Ni(III)/Ni(IV) Mixed Valence Ceramic Oxides

Though we did not succeed in preparing $SrLaNiO_{4-\delta}$ without oxygen deficiency and hence nickel appeared with an average oxidation state <3 (Fig. 6, $\delta \approx 0.05$), it is possible to synthesize mixed crystals $La_{1-x}Sr_xNiO_{4-\delta}$ with mostly $\delta \approx 0$ in the concentration range $0 < x \lesssim 0.5$ as pure well-defined black compounds, containing up to 40 mole% Ni(IV) (Table 1). These results confirm those of a detailed study, performed by Cava *et al.* (24) on the

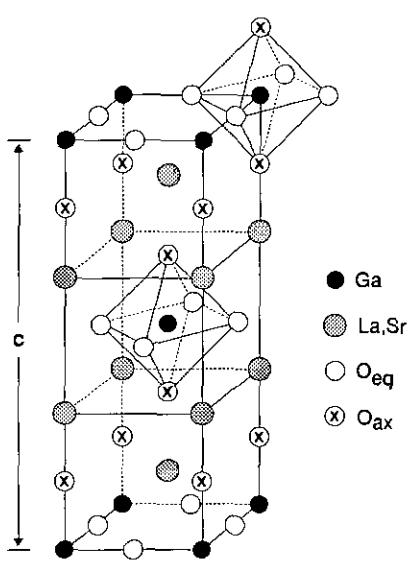

FIG. 11. The K_2NiF_4 structure of $SrLaGaO_4$.

TABLE 1

Unit Cell Constants (Å) of Mixed Valence K_2NiF_4-Type Compounds $Sr_{1+x}La_{1-x}NiO_{4-\delta}$ and Oxidation States (Ox) of Nickel in These Compounds

x	a	c	Ox	2δ
0	3.824	12.45	2.9	0.1
0.1	3.828	12.37	3.0	0.1
0.2	3.829	12.345	3.2	0
0.3	3.831	12.35	3.3	0
0.3[a]	3.828	12.34	3.15	0.15
0.4	3.833	12.36	3.4	0

[a] Different preparation.

same system. Apparently Ni(+IV) is stabilized by strong electronic interactions between the nickel centers inducing broad band behavior. This view is supported by looking at the a lattice constant which does not change significantly with x. In a local description Ni^{4+} is expected to have a low-spin t_{2g}^6 configuration due to a strongly enhanced $\Delta/B(C)$ ratio compared to Ni^{3+} and hence a considerably smaller ionic radius, in contrast to the experimental finding. Probably the positive hole is predominantly located on the oxygen ligands in a similar way to that proposed for Cu(III) in the superconducting mixed valent copper oxide ceramics (3, 24). Magnetic and electrical resistivity measurements give no indications of superconductivity in the temperature range down to 4 K (24, 25).

IV. SUMMARY

1. Various oxidic manganese(III) compounds with the perovskite and K_2NiF_4 structure were synthesized. In particular, if the Mn^{3+} ions are separated from each other in ordered lattices (e.g., elpasolite structure) there is clear evidence of distinct vibronic coupling effects of the Jahn-Teller type (strongly elongated MnO_6 octahedra). If the Mn^{3+} ions occur in clusters, electronic interactions between the paramagnetic centers lead to a broadening of the electronic levels, usually without being distinct enough to suppress the Jahn-Teller coupling, however. A further enhanced electron delocalization by introducing Mn^{4+} with a more pronounced covalency into the lattice—as in the K_2NiF_4-type mixed crystals $Sr_{1+x}Nd_{1-x}MnO_4$—introduces broad band behavior and reduces and finally completely suppresses the Jahn-Teller effect. Possibly this is one major reason why mixed valent Mn^{3+}–Mn^{4+} ceramic oxides do not exhibit superconductivity. In contrast Cu^{2+} fully preserves its vibronic coupling properties in the Cu(II)/Cu(III) superconductors.

2. Ni^{3+} can be stabilized in oxidic solids with the K_2NiF_4 structure, though Ni^{2+} is also present in varying concentrations. Isolated Ni^{3+} ions possess the low-spin configuration, which switches to the high-spin state, however, as soon as cooperative interactions between the nickel centers become important. The low-spin Ni^{3+} ions induce the expected Jahn-Teller polyhedron distortion. It is also possible to prepare mixed valence Ni(III)/Ni(IV) solids as pure compounds $Sr_{1+x}La_{1-x}NiO_{4-\delta}$ ($0 < x \lesssim 0.5$, $\delta \in 0$). Apparently Ni(IV) is stabilized by the already existing band structure of the nickel centers in $SrLaNiO_{4-\delta}$, possibly with the positive hole predominantly on the oxygen ligands. One reason why superconductivity is not observed might be the absence of low-spin Ni^{3+} in concentrated nickel oxide ceramics. The vibronic coupling in the octahedral E_g ground state, which determines the stereochemistry and the ground state of Cu^{2+} and also of low-spin Ni^{3+}, seems to play an important role in the superconductivity mechanism.

ACKNOWLEDGMENT

We owe thanks to Professor Yu. V. Yablokov (Kazan, GUS) for discussions on nickel ceramics during his stay in Marburg (financial support by DAAD).

REFERENCES

1. J. G. Bednorz and K. A. Müller, *Z. Phys. B* **64,** 189 (1986).
2. D. Reinen, Lecture presented at the German Inorganic Chemistry Meeting, Potsdam (Berlin), October 1994.
3. D. Reinen and J. Wegwerth, *Physica C* **183,** 261 (1991), and cited references therein.
4. G. C. Allen and K. D. Warren, *Struct. Bonding* **9,** 49 (1971).
5. D. Reinen, C. Friebel, and V. Propach, *Z. Anorg. Allg. Chem.* **408,** 187 (1974).
6. D. Reinen and C. Friebel, *Struct. Bonding* **37,** 1 (1979).
7. P. Köhler, W. Massa, D. Reinen, B. Hofmann, and R. Hoppe, *Z. Anorg. Allg. Chem.* **446,** 131 (1978).
8. R. D. Shannon, *Acta Crystallogr. Sect. A* **32,** 751 (1976).
9. G. Bayer, *Fortschr. Mineral.* **46,** 42 (1969).
10. G. Blasse, *J. Inorg. Nucl. Chem.* **27,** 993 (1965).
11. D. Reinen and M. Atanasov, *Magn. Reson. Rev.* **15,** 167 (1991).
12. K. H. Höck, H. Nickisch, and H. Thomas, *Helv. Phys. Acta* **56,** 237 (1983).
13. D. Reinen, *Theoret. Chim. Acta* **5,** 312 (1966).
14. ASTM No. 24-1191 (1989); Ref.: Gooden, McCarthy, JCPDS, Grant-in-Aid Report (1972).
15. K. Sander, U. Lehmann, und Hk. Müller-Buschbaum, *Z. Anorg. Allg. Chem.* **480,** 153 (1981).
16. (a) ASTM No. 24-1222 (1989); Ref.: Mizutani *et al., J. Chem. Soc. Jpn. Ind. Ed.* **73,** 1097 (1970). (b) D. Balz and K. Plieth, *Z. Elektrochem.* **59,** 545 (1955).
17. Z. Jirák, J. Wegwerth, and D. Reinen, to be published.
18. D. Belder, diploma thesis, Marburg 1991.
19. G. Demazeau, J. L. Marty, M. Pouchard, T. Rojo, J. M. Dance, and P. Hagenmüller, *Mater. Res. Bull.* **16,** 47 (1981).
20. W. Pietzuch, G. Berghöfer, U. Kesper, and D. Reinen, to be submitted.
21. Yu. V. Yablokov, T. A. Ivanova, S. Yu. Shipunova, N. V. Chezhina, I. A. Zvereva, and N. P. Bobrysheva, *Appl. Magn. Reson.* **2,** 547 (1991); T. A. Ivanov, E. F. Kukuvitskii, A. E. Usachev, and Yu. V. Yablokov, *Superconduct.* **5,** 861 (1992).
22. Work performed in cooperation with Yu. V. Yablokov.
23. J. D. Jorgensen, B. Dabrowski, Shiyon Pei, D. G. Hinks, L. Soderholm, B. Morosin, J. E. Schirber, E. L. Venturini, and D. S. Ginley, *Phys. Rev. B* **38,** 11,337 (1988).
24. R. J. Cava, B. Batlogg, T. T. Palstra, J. J. Krajewski, W. F. Peck, Jr., A. P. Ramirez, and L. W. Rupp, Jr., *Phys. Rev. B* **43,** 1229 (1991).
25. K. Sreedhar and J. M. Honig, *J. Solid State Chem.* **111,** 147 (1994).